Proceedings of ICFDP7:
7th International Congress on Fluid Dynamics and Propulsion
December 18-20, 2001, Cairo, Egypt

ICFDP7-2001047

AEROACOUSTICAL COMPUTATIONS OF UNSTEADY FLOWS AROUND A CIRCULAR CYLINDER

I. Pantle
Fachgebiet
Strömungsmaschinen
Universität Karlsruhe
Kaiserstraße 12
76128 Karlsruhe, Germany

F. Magagnato
Fachgebiet
Strömungsmaschinen
Universität Karlsruhe
Kaiserstraße 12
76128 Karlsruhe, Germany

M. Gabi
Fachgebiet
Strömungsmaschinen
Universität Karlsruhe
Kaiserstraße 12
76128 Karlsruhe, Germany

ABSTRACT

Growing environmental and energy saving consciousness increased the efforts to reduce penetrating sound emissions of machinery and technical constructions. Pre-design sound prediction methods are applied to avoid costly noise reduction treatment later on. Current prediction methods are mainly experimental and empiric or half-empiric solutions. This paper describes a numerical prediction method based on Computational Fluid Dynamics (CFD) and Acoustic Analogy. The method's main application field will be the computation of fan sound emission. In this context advantages and disadvantages in relation to other numerical methods (e.g. CFD/Linearized Euler Equations) will be pointed out.

The method is implemented into the department's own research CFD code. The parallelized, compressible code is able to do 2- and 3-dimensional unsteady Reynolds Averaged Navier-Stokes (RANS) as well as Large Eddy Simulations (LES). The acoustical module is based on the Ffowcs-Williams Hawkings equation. It extracts all necessary information out of the unsteady CFD computation, performs the Ffowcs-Williams Hawkings integration and computes density fluctuations, sound pressure levels and frequency spectra.

An unsteady, turbulent flow ($Re \approx 60{,}000$) around a circular cylinder was chosen as test case. The corresponding mesh was designed for unsteady turbulent (RANS and LES) 2- and 3-dimensional computations. For 3-dimensional computations this mesh was extended by copying the 2-dimensional plane 64 times into the third dimension. The acoustical frequency spectra of these turbulent flow computations are compared to experiments.

INTRODUCTION

During the last decades a lot of effort is taken to reduce penetrating sound emissions. Sources are considered penetrating when emitting permanently tonal sound components. Fans in air-conditioning systems are likely to emit penetrating noise due to their geometrical complexity: Though fans already have undergone a suitable noise reduction, they interact with the rotating and steady elements of the surrounding construction leading to a considerable noise emission. Currently available sound prediction methods still are not able to prevent unexpected noise behavior of such complex systems. In turn adding noise damping utilities after the installation is usually costly coming along with an additional demand of energy and space.

Therefore more and more attention is paid on the development of noise prediction methods for complex geometries. Numerical methods might replace a huge part of the state-of-the-art empirical methods as soon as time consumption and expenses reduce and as long as there is no significant loss in computational accuracy. The latter is required to resolve acoustical fluctuations which are some powers of 10 smaller than fluid flow fluctuations.

Mainly two numerical methods for acoustical computations are in development:

- A combination of CFD and Linearized Euler Equations (LEE): The fluid flow data required for acoustical computations will be extracted out of a CFD computation and given as input to an acoustical procedure solving the LEE in the acoustical computing domain [1].
- A combination of CFD and one form of the Acoustical Analogies (AA): The fluid flow data will be extracted out of a CFD computation and given as input to an acoustical procedure based on AA.

AA are solutions of the inhomogeneous, acoustic wave equation. These solutions appear in the form of one or more integrals. The first AA was derived by Lighthill 1952 [2]. The method described within this paper is an implementation of one form of the AA, which was derived by Ffowcs Williams and

Hawkings (FW-H) [3]. The following paragraphs describe the fundamentals of the method, show first test results and give an overview of possibilities and limitations of this method.

NOMENCLATURE

Indices	
d	drag
i,j,k	components of vectors
l	lift
p	sound pressure
Latin symbols	
$\boldsymbol{A}$	acceleration vector of a sound source [m s^{-2}]
c_0	speed of sound [m s^{-1}]
d	cylinder diameter [m]
e_{ij}	viscous stress tensor
f	frequency [Hz] (also force components f_i)
k	acoustic wave number [m^{-1}]
$\boldsymbol{M}$	Mach vector of a sound source
p	pressure [Pa]
p_0	reference pressure, static pressure [Pa]
$\boldsymbol{R}$	distance vector observer-source $\|\boldsymbol{x}$-$\boldsymbol{y}\|$ [m]
Re	Reynolds number
St	Strouhal number
T_{ij}	Lighthill's stress tensor
t	observer time variable [s]
$\boldsymbol{V}$	velocity vector of a sound source [m s^{-1}]
υ	velocity [m s^{-1}]
υ'	fluctuation of velocity [m s^{-1}]
$\boldsymbol{x}$	vector of observer position [m]
$\boldsymbol{y}$	vector of source position [m]
Greek symbols	
δ_{ij}	Kronecker delta
ρ	density [kg m^{-3}]
ρ_0	density of undisturbed flow [kg m^{-3}]
ρ', $\Delta\rho$	acoustical density fluctuation [kg m^{-3}]
μ_l	laminar viscosity [kg m^{-1} s^{-1}]
μ_t	eddy viscosity [kg m^{-1} s^{-1}]
τ	source emission time variable [s]
τ_e	source emission point of time [s]
ω	radiant velocity [s^{-1}]
ξ	relative vector of source position (moved system) [m]
θ	angle between $\boldsymbol{V}$ ($\boldsymbol{M}$) and $\boldsymbol{R}$

Missing symbols will be explained close to their appearance.

METHOD DESCRIPTION

The Acoustical Method

The acoustical method is based on the computation of the FW-H integral [3], using data extracted from CFD computations. The FW-H integral is a solution of the inhomogeneous wave equation (1) describing the propagation of acoustical waves through media with acoustical sources such as turbulent flows [4]. The first solution derived by Lighthill [2-5] considered the sources as mainly generated by turbulent and viscous effects. These were described by Lighthill's stress tensor T_{ij} including the viscous stress tensor e_{ij}:

$$\frac{\partial^2 \rho'}{\partial t^2} - c_0^2 \Delta \rho' = \frac{\partial^2 T_{ij}}{\partial x_i \partial x_j} \tag{1}$$

$$T_{ij} = \rho \overline{\upsilon_i' \upsilon_j'} + \delta_{ij}[(p - p_0) - c_0^2(\rho - \rho_0)] - e_{ij} \tag{2}$$

$$e_{ij} = \mu_l \cdot \left(\frac{\partial \upsilon_i}{\partial x_j} + \frac{\partial \upsilon_j}{\partial x_i} - \frac{2}{3}\delta_{ij} \frac{\partial \upsilon_k}{\partial x_k} \right) \tag{3}$$

Subsequent solutions as the Ffowcs Williams and Hawkings Acoustic Analogy show different interpretations of the source term on the right hand side of the wave equation. Each interpretation contains Lighthill's stress tensor T_{ij}. The product $\rho \overline{\upsilon_i' \upsilon_j'}$ can be interpreted as the turbulent stress tensor being modeled in turbulence modeling. Eddy viscosity models typically set up the following relationship:

$$\rho \overline{\upsilon_i' \upsilon_j'} = \mu_t \cdot \left(\frac{\partial \upsilon_i}{\partial x_j} + \frac{\partial \upsilon_j}{\partial x_i} - \frac{2}{3}\delta_{ij} \frac{\partial \upsilon_k}{\partial x_k} \right) \tag{4}$$

with the eddy viscosity μ_t. Primed symbols represent fluctuations of the mean flow values.

The Ffowcs Williams and Hawkings source terms take into account the effects of pressure fluctuations, hard walls and geometry thickness on the sound emission [6].

$$\begin{aligned}
&\rho'(\boldsymbol{x},t) = \\
&= \frac{1}{4\pi c_0^2} \frac{\partial^2}{\partial x_i \partial x_j} \int_{v(\tau_e)} \left[\frac{T_{ij}}{R\left|1 - (\boldsymbol{R}/R)\boldsymbol{M}\right|} \right]_{\tau=\tau_e} d\xi \\
&- \frac{1}{4\pi c_0^2} \frac{\partial}{\partial x_i} \int_{S(\tau_e)} \left[\frac{f_i}{R\left|1 - (\boldsymbol{R}/R)\boldsymbol{M}\right|} \right]_{\tau=\tau_e} dS(\xi) \\
&- \frac{1}{4\pi c_0^2} \frac{\partial}{\partial x_j} \int_{v_c(\tau_e)} \left[\frac{\rho_0 A_j}{R\left|1 - (\boldsymbol{R}/R)\boldsymbol{M}\right|} \right]_{\tau=\tau_e} d\xi \\
&+ \frac{1}{4\pi c_0^2} \frac{\partial^2}{\partial x_i \partial x_j} \int_{v_c(\tau_e)} \left[\frac{\rho_0 V_i V_j}{R\left|1 - (\boldsymbol{R}/R)\boldsymbol{M}\right|} \right]_{\tau=\tau_e} d\xi
\end{aligned} \tag{5}$$

This form of the FW-H integral is valid in the whole space and gives the density fluctuations at an observer point $\boldsymbol{x}$ in the inertial system and at the observer time t: $\rho' = \rho'(\boldsymbol{x},t)$. The position of a source in the inertial system is described by $\boldsymbol{y} = (\xi,\tau_e)$ depending on the source's relative coordinates in the moved system ξ (source volume element $d\xi$) and the emission time τ. The integration domain $v(\tau)$ describes a flow volume

including an acoustical source, $v_c(\tau)$ describes a volume in the flow without flow going through, e.g. some hard walled geometry dragging the flow around, enclosed within the surface $S(\tau)$. The surface $S(\tau)$ exerts viscous and pressure forces contributing to the sound generation: $f_i = -n_i(p - p_0) + n_j e_{ij}$.

The thickness of the volume $v_c(\tau)$ has additional effects on the fluid through its own velocity $\boldsymbol{V}(\tau)$ and acceleration $\boldsymbol{A}(\tau)$ (Mach vector $\boldsymbol{M}(\tau)$). The distance for an acoustic signal to travel equals the distance between observer and source in the inertial system. Keeping the observer at constant position this distance depends on the source's position at emission time τ_e: $\boldsymbol{R}(\boldsymbol{\xi}, \tau_e) = \boldsymbol{x} - \boldsymbol{y}(\boldsymbol{\xi}, \tau_e)$.

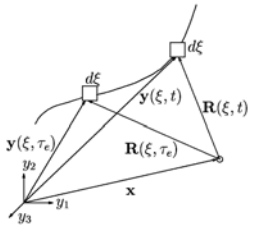

Fig. 1: Spatial scheme of moving acoustic sources

Figure 1 shows the relation of observer and source position schematically. Vector $\boldsymbol{R}$ is constant in the case of a non moving source ($\boldsymbol{M} = \boldsymbol{A} = 0$). In this case only the first two terms of the FW-H integral will be left and the observer will be able to receive an acoustic signal for spatially variable T_{ij} and/or f_i. The acoustical observer domain is considered independent of the source domain and can be included in or excluded from the source domain (the CFD domain) where pressure, viscous and turbulent information necessary for the summands of the FW-H integral is computed. The CFD domain extends into regions where acoustical sources can be considered weak and negligible.

Considering flow fans as the future object of studies the observer is expected to reside rather far outside the source/CFD domain. This in turn sets up two main restrictions: A good resolution of an acoustic wave requires a good resolution of the time period and the wave length. In terms of cell width for a numerical grid this is in the range of millimeters for audible frequencies whereas the observer might reside meters away. Resolving this distance represents a huge numerical effort and it should be taken into account if the aim of study requires the resolution of the whole acoustic domain or tends to examine only discrete observer points. For the first step of this implementation only discrete observer points were chosen. So the FW-H integral was taken in its farfield approximation:

$$\rho'(\boldsymbol{x}, t) \approx$$

$$\approx \frac{1}{4\pi c_0^4} \int_{v(\tau_e)} \left[\frac{R_i R_j}{R^3 \hat{C}} \cdot \frac{\partial}{\partial \tau} \frac{1}{\hat{C}} \frac{\partial}{\partial \tau} \frac{T_{ij}}{\left|\hat{C}\right|} \right]_{\tau=\tau_e} d\xi$$

$$+ \frac{1}{4\pi c_0^3} \int_{S(\tau_e)} \left[\frac{R_i}{R^2 \hat{C}} \cdot \frac{\partial}{\partial \tau} \frac{f_i}{\left|\hat{C}\right|} \right]_{\tau=\tau_e} dS(\xi)$$

$$+ \frac{1}{4\pi c_0^3} \int_{v_c(\tau_e)} \left[\frac{R_j}{R^2 \hat{C}} \cdot \frac{\partial}{\partial \tau} \frac{\rho_0 A_j}{\left|\hat{C}\right|} \right]_{\tau=\tau_e} d\xi$$

$$+ \frac{1}{4\pi c_0^4} \int_{v_c(\tau_e)} \left[\frac{R_i R_j}{R^3 \hat{C}} \cdot \frac{\partial}{\partial \tau} \frac{1}{\hat{C}} \frac{\partial}{\partial \tau} \frac{\rho_0 V_i V_j}{\left|\hat{C}\right|} \right]_{\tau=\tau_e} d\xi \qquad (6)$$

with the Doppler factor $\hat{C} = 1 - \frac{\boldsymbol{RM}}{R} = 1 - M \cdot \cos\theta$.

Spatial derivations can be transformed into time derivations throughout the farfield approximation [6]. This approximation is valid sufficiently far away from the source region. In the case of a non moving geometry ($\boldsymbol{M} = \boldsymbol{A} = 0$) only the first two terms will differ from zero and an observer receives acoustic signals exclusively when the acoustic sources T_{ij} and/or f_i are time dependent. In turn a steady state CFD solution only produces a signal at the observer position if the source region has an external velocity ($\boldsymbol{R} \neq const$). With the farfield approximation the problem of resolving the whole acoustic domain is obsolete and acoustic computations are reduced to discrete observer points. Still sufficient fine time steps are required.

Properties of the CFD Solver

The acoustical module was implemented into the research CFD solver SPARC which was developed at the Department of Fluid Machinery, University of Karlsruhe. This code is able to do 2- and 3-dimensional computations, based on the compressible Navier Stokes equations. It uses finite volumes and a multigrid method [7]. Turbulent flows can either be modeled with Reynolds Averaged Navier Stokes (RANS) equations selecting within several algebraic, one-equation, linear and non-linear two-equation models. It provides also the possibility to perform a Large Eddy Simulation (LES) [8-9].

The data of the CFD computation in each time step is taken as input to the acoustic module. According to the finite volume method the flow data is computed in the cell centers of the CFD domain. The acoustic module takes each cell as a compact sound source and performs the integration of the turbulent data within the cell volume. Consequently the signals of all sources travel to the observer and the signal recorded by the observer is a superposition of all these. So the acoustic module also sorts and superposes the emitted source signals according to their arrival time at the observer.

Possibilities and Limitations of the Described Method

The focus of this work is the creation of a tool for predicting the acoustical behavior of fluid machinery in complex geometries. Generally the CFD/LEE method is preferred for numerical acoustical schemes. There the acoustical information is computed in a discretized numerical domain not just at discrete observer points. Solving LEE also considers interactions between acoustical motion and flow motion. This is an advantage in comparison to the CFD/AA method. However, solving LEE represents still a much higher numerical effort especially in the case of complex 3-dimensional geometries. So present research works and experiences with CFD/LEE are almost exclusively done on airfoil and jet noise [1-10]. But CFD/LEE methods might become realizable also for fluid machinery as available computing resources improve.

The CFD/AA method in this paper is a farfield solution. The integral is valid outside the source region. Therefore examinations of the acoustical behavior inside the source region and of interactions between flow motion and acoustic motion in the source region are not possible. For fluid machinery this restriction is tolerable as observers typically reside outside this region.

Comparing the CFD/LEE and the CFD/AA method the latter requires a second order scheme for the flow computation [1] whereas CFD/LEE usually requires low dispersive schemes of at least fourth or higher orders. The turbulent data of the CFD/AA computation and its accuracy concerning also the acoustical results are expected to depend strongly on the applied modeling of the turbulent behavior. In the case of unsteady RANS modeling statistical averaging gives a characteristic turbulent energy spectrum. The frequencies resolved in this energy spectrum cover a small band, other frequencies are averaged out and cannot be resolved. In comparison LES resolves a much broader range of frequencies in this spectrum. Only the small scale structures are modeled containing a small percentage of the turbulent energy and covering the very high frequencies. The corresponding frequencies there are mostly averaged out as in the case of unsteady RANS. This is subject for further studies.

Concerning computational resources the CFD/AA method presently requires a plus of memory of about 10 % in comparison to a pure CFD computation. Within one time step of CFD computation the plus of required cpu time is negligible. However, presently a minimum of about 1,000 time steps is needed to perform a reasonable Fourier transformation with about 50 time steps per period. This requires a computation of about 20 cycles whereas a pure CFD computation is usually performed within about 10 cycles.

TEST CASE

General Considerations

As validation test case for the acoustical method a flow around a circular cylinder was chosen. This serves as a 2-dimensional case as well as a 3-dimensional one. The unsteady flow develops a vortex street behind the cylinder. It is caused by pressure fluctuations on the cylinder surface, inducing lift and drag force fluctuations. In the laminar case (for Reynolds numbers up to $Re \approx 250$) the von Karman vortex street will be rather regular over a long distance after the cylinder with a row of vortices of alternating rotation [11]. The lift force fluctuation is oscillating with the lowest and fundamental frequency, the drag force fluctuation with the first harmonic.

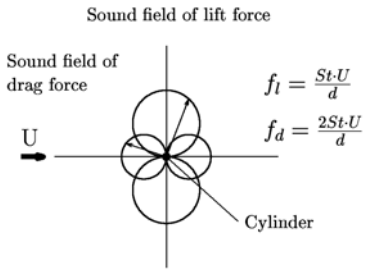

Fig. 2: Direction dependency of the sound field of aeolian tones, Etkin et al. [12]

These fluctuations generate the so-called aeolian tones with the same frequencies. A frequency spectrum is expected to show clearly two dominant peaks at the fundamental and first harmonic frequency. According to Etkin et al. [12] these acoustic oscillations are considered dipoles emitting sound with characteristic direction dependencies: The lift force fluctuations are expected to emit the highest intensity along the directions perpendicular to the flow (and the cylinder), the drag force fluctuations along the flow direction.

Figure 2 shows this behavior schematically in a 2-dimensional plane with the cylinder as dot in the center of the coordinate system. The main frequencies of the emitted sound waves can be determined by the Strouhal number $St = f\,d/U$ of the considered problem. The Strouhal number is a function of the Reynolds number Re. For Reynolds numbers lower than $Re \approx 200$ the Strouhal number grows with increasing Reynolds number. For higher Reynolds numbers ($Re \leq 10{,}000$) the Strouhal number reaches a plateau. Empirically this is determined to be in the range of $0.18 \leq St \leq 0.22$. With further increasing Re again St shows a dependency of Re [12].

In the turbulent case the vortex street develops less regularly than in the laminar case. Consequently it is expected that more frequencies appear in the upper range of the frequency spectrum though the frequencies of lift and drag force fluctuations should have the same dominant peaks.

Turbulent Flow around a Circular Cylinder

Etkin et al. performed experiments in the turbulent flow region [12]. As mentioned the acoustical frequency spectrum of the computation is expected to show some noise due to turbulent sources entering the acoustical computation. However, performing unsteady RANS will not resolve a broad

range of frequencies. Still the fundamental frequency should be clearly visible in the following configuration with the observer at distance of 0.6 m perpendicular to the main flow direction under the cylinder whereas the first harmonic should not.

For the 2- and 3-dimensional flow computations the following settings were identical: The main flow velocity was U = 68.625 m/s, giving a Mach number of Ma =0.2, the cylinder diameter was $d = 1.25 \cdot 10^{-2}$ m. The flow medium was air at environmental temperature, the Reynolds number computed with the cylinder diameter was Re = 60,000. The unsteady computation was performed using the k-τ-model of Speziale, Abid and Anderson [13]. The turbulence level was set according to results of Etkin et al. to 0.3 % [12]. For the turbulent computation also some information about turbulent length scale or eddy viscosity is required which cannot be found in the experimental description. So as starting value a reasonable eddy viscosity ratio was chosen. Due to previous computing experiences it was set to $\mu_t / \mu_l = 1.0$.

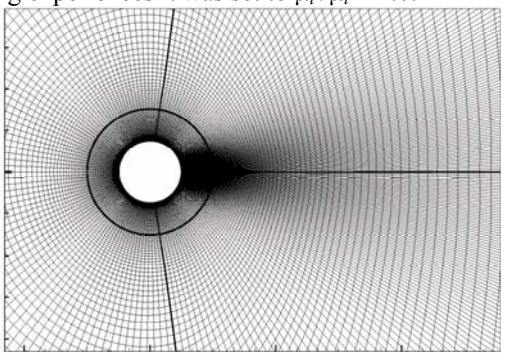

Fig. 3: Numerical mesh (2D plane)

The computational schemes were of second order accuracy both in space and time. The numerical mesh consisted of about 50,000 cells (figure 3). The 2-dimensional mesh showed a distance between the cylinder and the mesh boundary of about 17 diameters in the upstream direction, 20 diameters in the directions perpendicular to the flow and 43 diameters downstream. At the boundaries upstream and parallel to the flow a farfield condition was applied, downstream the static pressure was set. In the third direction (along the cylinder) there was a symmetry condition. The time steps used for the acoustical computation were $\Delta t = 2 \cdot 10^{-5}$ s.

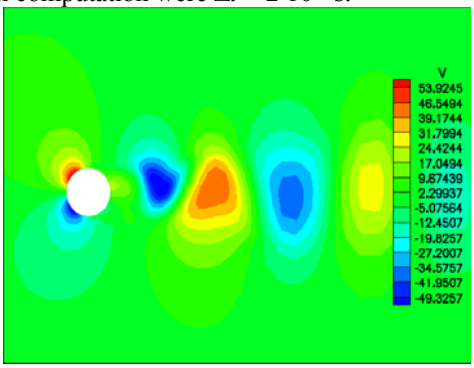

Fig. 4: Moment shot of the velocitiy component υ perpendicular to the main flow

The Strouhal number of the monitored lift fluctuation was determined to be 0.213, corresponding to a fundamental frequency of f = 1,172 Hz. The frequency step of the computed narrow band sound pressure level spectrum $PSDL_p$ (Power Spectral Density Level of pressure) was constant $\Delta f \approx 24$ Hz. The fundamental frequency was determined to be f = 1,190 Hz (St = 0.217).

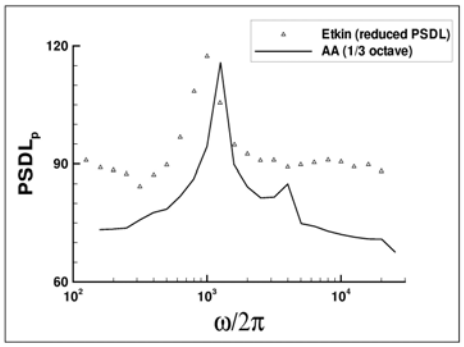

Fig. 5: Power spectral density level of sound pressure (third octave spectrum); 2D-URANS; observer position at (0, 0.6)

Figure 5 shows the third octave spectrum including the results of Etkin et al. Their results are plotted as a noise reduced $PSDL_p$-curve. The first harmonic is not visible in this spectrum neither in the results of Etkin et al. nor in the numerical ones. The second harmonic instead is visible in the numerical results but invisible in the ones of Etkin et al. Also the main peaks differ in their position: Etkin et al. found the main peak in the third octave band of f = 1,000 Hz whereas the numerical main peak is in the next higher band of f = 1,250 Hz. These third octave bands share the border at f = 1,122 Hz corresponding to a Strouhal number of St = 0.20. Etkin et al. do not mention the exact Strouhal number of the configuration here taken. Though the numerically determined one seems slightly higher than the one of Etkin et al., however it still resides in the empirically determined range for these cylinder flow configurations. The main peak of Etkin et al. shows a $PSDL_p$ of 117 dB which is theoretically underestimated. Etkin et al. expected it to be at about 124 dB in theory. The computational result of 116 dB corresponds very much to the experimental one.

The 2-dimensionality of this first computation implies that the amplitude and the phase of the oscillating forces are assumed constant over the cylinder length, which is possible only over a correlative cylinder length of a maximum of four cylinder diameters, neglecting end effects [6]. The flow values in this 2-dimensional computations are normalized to unit length. The experimental setup exceeds with a cylinder length of 0.8 m the correlative length by far. However, Etkin at al. treat their experiment as 2-dimensional but do not give a correlative length. This might have misleading effects on the comparison with the computational results.

Though the experimental curve in figure 5 was reduced about the noise level of the experimental setup it still shows a very high background level. Especially in the high frequency range Etkin et al. explain this as the random turbulent quadrupole sources. These cannot be resolved with this unsteady but RANS modeled computation. A 3-dimensional LES might lead to better results here. Though this was a turbulent computation still the effect of the turbulent sources T_{ij} in comparison to the sources resulting from the forces f_i has not yet been studied.

A preliminary 3-dimensional computation with unsteady RANS was performed, using the same configuration as in the 2-dimensional case. In the third dimension the mesh spanned 3 cylinder diameters with 64 cells. The total amount of cells was about 3,000,000. The boundary conditions of the third dimension were periodic. However, this computation was performed in a coarser grid of about 50,000 cells. Since in 3-dimensional computations the acoustical density fluctuations close to the symmetry plane of the cylinder are directly proportional to the cylinder length ([6], [12]) the computational results need to be normalized to the experimental cylinder length for a better comparison. Figure 6 shows the normalized computational $PSDL_p$-curve.

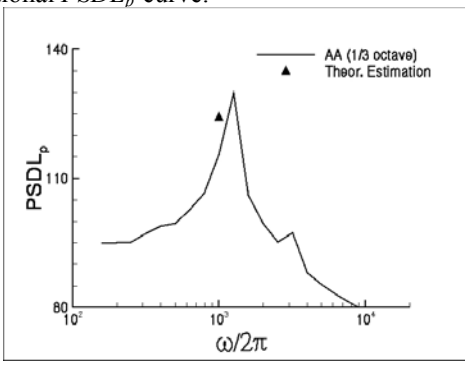

Fig. 6: Power spectral density level of sound pressure (third octave spectrum); 3D-URANS; observer position at (0, 0.6, 0.01875)

The numerical peak positions in the 3-dimensional case agree with those of the 2-dimensional case although the height of the main peak exceeds the 2-dimensional one. Etkin et al. estimated a theoretical peak height of about 124 dB at their main frequency f = 1,000 Hz but treated their experiment 2-dimensionally. The computational peak height of 129 dB in this coarse grid is considerably higher but is expected to fall with changing to a finer grid because of typically decreasing amplitudes of the forces' fluctuations in finer grids. As expected the first harmonic is not visible, but as in the 2-dimensional case the second harmonic is of considerable height.

SUMMARY

This paper described a numerical method to compute sound emission. The method uses Acoustical Analogy within a CFD solver. Advantages and disadvantages of the CFD/AA combination in the context of performing fluid flow computations for complex, 3-dimensional geometries were shown. A 2- and a 3-dimenional test case were presented. They were taken from the experiments of Etkin et al. [12]. The results seem promising but require further studies: The main peaks' sound pressure level in the 2-dimensional case agrees well with the experimental one. In the 3-dimensional case it seems far too high but is expected to fall with further computations in finer meshes. The peak positions in the numerical frequency spectra coincide but differ from the experimental one. This might result from a numerical over-estimation of the Strouhal number and is therefore subject for further studies.

Examinations were done with unsteady RANS. Since it is expected that LES will lead to more accurate acoustical results performing an LES will be the next step. This method was chosen for the computation of complex geometries, so finally flow fans shall be tested and the results included in the department's fan research projects.

REFERENCES

[1] R. R. Mankbadi. *Transition, Turbulence and Noise: Theory and Applications for Scientists and Engineers.* Kluwer Academic Publishers, 101 Philip Drive, Assinippi Park, Norwell, Massachusetts 02061, USA, 1994.

[2] M. J. Lighthill. On sound generated aerodynamically. I. General theory. *Proc. Roy. Soc. (London)*, 211(A):564-587,1952.

[3] J. E. Ffowcs Williams and D. L. Hawkings. Sound generation by turbulence and surfaces in arbitrary motion. *Phil. Trans. Roy. Soc. (London)*, 264(A):321-342,1969.

[4] A. Hirschberg and S. W. Rienstra. *An introduction to Acoustics.* Intituut Wiskundige Dienstverlening Eindhoven, Eindhoven, NL, 1997.

[5] M. J. Lighthill. On sound generated aerodynamically. II. Turbulence as a source of sound. *Proc. Roy. Soc. (London)*, 222(A):1-34,1954.

[6] Marvin E. Goldstein. *Aeroacoustics.* McGraw-Hill, Inc., USA, 1976.

[7] F. Magagnato. Kappa – KArlsruhe Parallel Program for Aerodynamics. *TASK Quarterly – Scientific Bulletin of Academic Computer Center in Gdansk*, 2(2):215-270, 1998.

[8] F Magagnato. Unsteady flows past a turbine blade using a non-linear two-equation turbulence model. *3rd European Conference of Turbomachinery: Fluid Dynamics and Thermodynamics*, 1999.

[9] F. Magagnato and M. Gabi. A new adaptive turbulence model for unsteady flow fields in rotating machinery. *International Journal of Rotating Machinery*, 2000.

[10] V. Fortuné and Y. Gervais. Numerical investigation of noise radiated from hot supersonic turbulent jets. *AIAA Journal*, 37(9):1055-1061, 1999.

[11] M. M. Zdravkovich. *Flow around Circular Cylinders Vol1: Fundamentals.* Oxford University Press, Oxford, GB, 1997.

[12] B. Etkin, G. K. Korbacher, R. T. Keefe. Acoustic radiation from a stationary cylinder in a fluid stream (aeolian tones). *Journal of the Acoustical Society of America*, 29:30-36, 1957.

[13] C. G. Speziale, R. Abid and E. C. Anderson. A critical evaluation of two-equation models for near wall turbulence. *ICASE Report*, No. 90-46, 1990.